ADVANCED MATERIALS
www.advmat.de

Mechanism of Hot-Carrier Photoluminescence in Sn-Based Perovskites

*Eelco K. Tekelenburg, Franco V. A. Camargo, Alessio Filippetti, Alessandro Mattoni, Larissa J. M. van de Ven, Matteo Pitaro, Giulio Cerullo, and Maria A. Loi**

Metal halide perovskites have shown exceptionally slow hot-carrier cooling, which has been attributed to various physical mechanisms without reaching a consensus. Here, experiment and theory are combined to unveil the carrier cooling process in formamidinium (FA) and caesium (Cs) tin triiodide thin films. Through impulsive vibrational spectroscopy and molecular dynamics, much shorter phonon dephasing times of the hybrid perovskite, which accounts for the larger blueshift in the photoluminescence seen at high excitation density for $FASnI_3$ compared to $CsSnI_3$ is reported. Density functional theory investigations reveal that the largest contribution to the blueshift is accounted by a giant, dynamic band-filling effect in Sn-based perovskites, which in turn can explain the cooling disparity with the Pb-based counterparts. Several years after the first experimental observations, here a deeper understanding of the cooling mechanism of these materials is provided. Design principles for hot-carrier materials, which may be useful for future implementations of hot-carrier solar cells are further provided.

1. Introduction

Hot carriers are defined as carriers with a temperature higher than the lattice temperature, i.e. carriers with energy in excess with respect to their band energies at equilibrium occupancy. A material showing slow cooling of hot carriers could be technologically and economically interesting as its application in solar cells would allow to exceed the detailed balance limit of 33%.[1] Whereas traditional inorganic semiconductors show cooling within 1 ps, i.e. too fast for practical device purposes, metal halide perovskites have shown exceptionally slow cooling of up to several nanoseconds at high excitation densities.[2] This feature has stimulated an intense scientific effort in an attempt to understand the underlying principles.[2–9] As many of the unique properties of metal halide perovskites stem from the interaction of charge carriers with the soft deformable ionic lattice, it is also in this case a common belief that electron-phonon coupling is at the origin of the slow cooling of hot carriers.[3–5,10,11]

The ionic lattice of metal halide perovskites is denoted by the chemical formula ABX_3. A is a small monovalent cation, typically formamidinium (FA), methylammonium (MA), or caesium (Cs). B is a divalent metal cation such as Pb or Sn, and X is a halide anion. It has become clear that the composition of the perovskites largely influences the time scale of the cooling dynamics, although the physical reasons behind this effect remain controversial.[11,12] Several studies have shown the importance of the small organic cation to prolong the cooling of hot carriers,[13] which was associated with a phonon mode of the organic cation,[4,5] while others reported a faster cooling for the organic cations due to the higher phonon density of states.[8] Changing Pb with Sn was also shown to further extend the cooling time from hundreds of picoseconds to several nanoseconds at high excitation densities.[2,12] This scenario makes Sn-based perovskites extremely promising hot-carrier materials.

An in-depth understanding of the phonon modes is vital to comprehend the cooling dynamics. A powerful measurement technique to study these modes in real time is impulsive vibrational spectroscopy (IVS), which allows for retrieving coherent phonon oscillations from transient absorption spectra.[14] The application of this technique to layered and 3D perovskites has led to an increased understanding of the exciton-phonon and carrier-phonon interactions.[15–18] For example, it was found that

E. K. Tekelenburg, L. J. M. van de Ven, M. Pitaro, M. A. Loi
Zernike Institute for Advanced Materials
University of Groningen
Nijenborgh 4, 9747 AG Groningen, The Netherlands
E-mail: m.a.loi@rug.nl
F. V. A. Camargo, G. Cerullo
Istituto di Fotonica e Nanotecnologie-CNR
Piazza Leonardo da Vinci 32, Milano 20133, Italy
A. Filippetti
Dipartimento di Fisica
Università di Cagliari
S.P. Monserrato-Sestu Km. 0700, Monserrato, CA 09042-I, Italy
A. Filippetti, A. Mattoni
Consiglio Nazionale delle Ricerche
Istituto Officina dei Materiali, CNR-IOM, Cagliari
Cittadella Universitaria
Monserrato, CA 09042-I, Italy
G. Cerullo
Dipartimento di Fisica
Politecnico di Milano
Piazza L. da Vinci 32, Milano 20133, Italy

The ORCID identification number(s) for the author(s) of this article can be found under https://doi.org/10.1002/adma.202411892

DOI: 10.1002/adma.202411892

coherent phonon dephasing is likely to originate from the decay of longitudinal optical phonons into two longitudinal acoustic phonons, rather than from scattering by defects.[17] In addition, it has been claimed that a phonon mode of 0.9 THz (30 cm^{-1}) could be at the origin of the phonon bottleneck in $MAPbI_3$.[18,19] However, to our knowledge, a direct analysis of how the measured phonon dephasing time relates to hot-carrier cooling in Sn-based perovskites has not been carried out so far.

In this work, we provide a fundamental understanding of the hot-carrier phenomenon through a combined experimental and theoretical analysis of electronic and vibrational properties of $FASnI_3$ and $CsSnI_3$ thin films. We furnish clear evidence that the type of A-site cation has a large impact on the phonon decay contributing to the hot-carrier photoluminescence (PL). On the other hand, the large blueshifts observed in the PL are chiefly the result of a giant dynamic Burstein–Moss effect, owing to the peculiarly low density of states (DOS) of the stannates at the band edges. This feature sets stannates and plumbates quite far apart and motivates the longer cooling time of the former. Importantly, our results suggest new design principles for the identification and implementation of viable hot-carrier materials.

2. Results

The schematic picture in **Figure 1a** depicts the cooling mechanism in semiconductors. After excitation with excess energy, charge carriers reside high in the electronic band. The excess energy is dissipated through the emission of longitudinal optical phonons, and charge carriers accumulate at the band edges.[11] The longitudinal optical phonons decay into acoustic phonons, which ultimately lead to the heating of the lattice.[11] Since cooling takes place through carrier-phonon scattering, it takes place as long as the probability of a carrier losing energy to a phonon is higher than that of gaining energy from it. Besides, electronic states at the lower energy must be available. These conditions are typically met only up to a certain carrier density, beyond which carrier excitation can lead to lingering hot carrier populations. If insufficient electronic states are available at the band extrema, phonons cannot be emitted and the electrons remain hot for a longer period of time due to Pauli blocking. This mechanism is highly enhanced in the condition of large band filling, i.e. large Burstein–Moss effect.[2,7,13] A band-filling regime is favored by a high doping density (static Burstein–Moss effect), a low DOS at the band edges, and a slow recombination rate (dynamic Burstein–Moss effect).[6,7,13,20–22]

If the probability of a carrier losing energy to a phonon is equal to gaining energy from it, we have what is referred to as a hot-phonon bottleneck. This can be reached in various ways; for example, in conventional inorganic quantum dots, quantization effects have been predicted to significantly reduce the scattering rate and prolong the lifetime of phonons due to a phonon bandgap.[23,24] In perovskites, it has been proposed that the phonon bottleneck can be created by long-lived optical phonons or by upconversion of acoustic phonons that efficiently reheat the charge carriers.[4,19,25] This is motivated by the peculiar features of the perovskite phonon band structure, characterized by optical frequencies compressed within a narrow, low-energy window partially overlapping with acoustic modes, thus favoring strong phonon reabsorption.[4] In conventional semiconductors

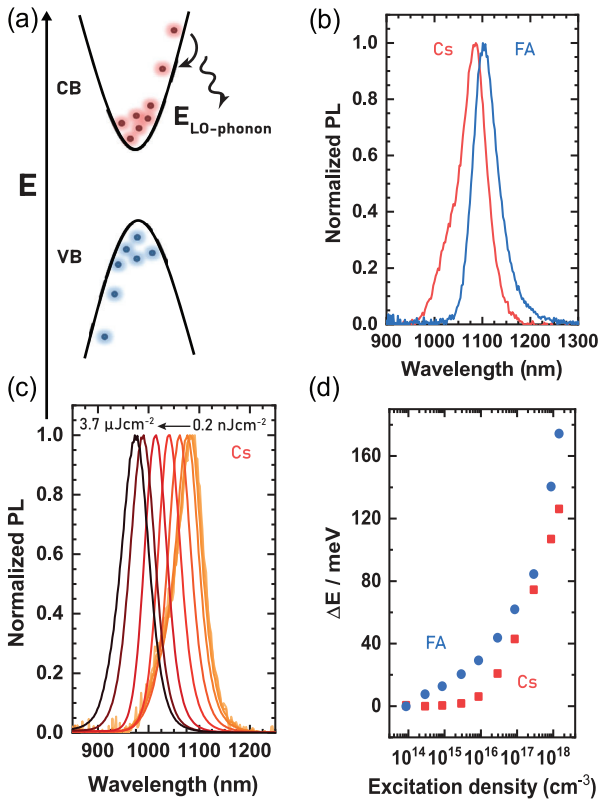

Figure 1. a) Schematic of hot-carrier cooling through the emission of longitudinal optical phonons and subsequent state filling at the band edge. b) Normalised PL spectra of $CsSnI_3$ and $FASnI_3$ using a fluence of 0.2 $nJcm^{-2}$ (≈8.6· 10^{13} cm^{-3}) at 4.4 K and c) with increasing fluence for $CsSnI_3$. d) The energy shift of the peak position as a function of excitation density at 4.4 K for both compounds.

(e.g. GaAs), on the other hand, optical modes are much higher in energy, such that, once emitted, they are quickly depopulated. In addition to electronic and phonon bottleneck mechanisms, the formation of polarons has also been reported as a possible cause of slow carrier cooling, based on the idea that the polaron–phonon interaction can be much weakened with respect to the bare electron–phonon coupling.[5]

In this study, thin films of $FASnI_3$ and $CsSnI_3$, prepared according to the details described in the Supporting Information, were used to elucidate the mechanism of hot-carrier cooling. We took great care in optimizing the deposition conditions for the thin films to the same level of defect density, as discussed in our previous work.[13] The PL spectra of $FASnI_3$ and $CsSnI_3$ at 4.4 K are shown in Figure 1b. The two compounds show similar emission features peaking at 1103 nm with a full width at half maximum (FWHM) of 64 nm for $FASnI_3$ and 1085 nm with a FWHM of 59 nm for $CsSnI_3$. The normalized PL with increasing excitation fluence is shown for $CsSnI_3$ in Figure 1c and shows that the peak position exhibits a pronounced blueshift up to 3.7 μJcm^{-2} (carrier density of ≈1.4×10^{18} cm^{-3}), indicative of a large contribution of hot-carrier PL.[2] Also, we observe a remarkable stability of $CsSnI_3$ at these high fluences, while $FASnI_3$ shows a slight broadening after high-fluence excitations - see Figure S1 (Supporting Information). The energy shift of the

peak is extracted from these spectra and compared with $FASnI_3$ in Figure 1d, see Figure S2 (Supporting Information) for PL spectra of $FASnI_3$. A striking similarity in the peak shifts of the compounds is obtained, where $FASnI_3$ exhibits only a larger shift compared to $CsSnI_3$. These shifts are much larger than the previously reported values for Pb-based systems and establish an unexpected difference for CsPb-based compositions reported by others.[2,5]

One might suggest that the origin of these shifts is related to defects as it is well-known that Sn-based perovskites are challenging to produce. However, we can exclude defects as it has been shown repeatedly that materials of lower quality show faster cooling and lower hot-carrier PL contribution instead.[3,26–28] It is therefore improbable that either disorder or defects in the band structure could trap carriers and thereby prolong the cooling.[6] At 4.4 K, one would expect charges to be trapped and additional states are expected to be resolved. The fact that we observe neither a second high-energy resonance nor a saturation of the blueshift with increasing fluence firmly excludes defects as a possible origin. In addition, the linear excitation fluence dependence of the PL intensity over more than three orders of magnitude also excludes Auger recombination being of importance in the cooling dynamics (Figure S3, Supporting Information).

Previous studies have reported the importance of phonons in the observation of long-lived hot carriers.[2–6,25] To understand the vibrational dynamics of tin-based perovskites, we performed impulsive vibrational spectroscopy - a technique based on transient absorption spectroscopy. **Figure 2a** shows the differential transmission (ΔT/T) of $FASnI_3$ (open circles) at two selected probe wavelengths at 5 K with a near-resonance pump of 980 nm (1.27 eV), see also Figure S4a (Supporting Information) for the transient absorption map. Positive values of ΔT/T correspond to reduced absorption of the sample due to the band filling of charge carriers near the band edge, also referred to as photobleaching.[7] The negative ΔT/T signal in the top panel has been attributed to photoinduced absorption bands and to changes to the refractive index.[29,30] A negative ΔT/T signal toward lower energies of the band edge is associated with bandgap renormalization due to electron and hole exchange correlations (Figure S4a, Supporting Information), which in our case quickly vanishes due to near-resonance excitation and carrier-carrier scattering.[3] A close inspection of the graphs in Figure 2a reveals modulations in the ΔT/T signal; a signature of coherent phonons impulsively excited by the pump pulse. The ΔT/T signal was globally fitted with exponential decays to account for the electronic population dynamics (full lines in Figure 2a).[31] The residuals of the fit, shown in Figure 2b, exhibit two vibrational modes: one mode with a period of ≈0.25 ps (133 cm^{-1}) and a lower frequency period of ≈1.3 ps (25 cm^{-1}), similar to the 23 cm^{-1} mode observed in $MAPbI_3$.[32] In Figure S4b (Supporting Information) a node is observed close to the bleach peak maximum, where the amplitude of the oscillations on the blue side of the node is in anti-phase with the amplitude on the red side. This is evidence that the 133 cm^{-1} mode is generated through impulsive stimulated Raman scattering.[14,15]

To retrieve the dephasing time of the coherent modes, we fitted the residuals using a damped oscillatory function:

$$f(t) = Ae^{-\frac{t}{\tau}}\sin(\omega t - \phi) + y_0 \quad (1)$$

where A is the amplitude, τ the dephasing time, ω the frequency, ϕ the phase, and y_0 the offset. We note that coherent interactions between pump and probe pulses during their temporal superposition - not taken into account in the fitting of the population dynamics - can introduce artefacts in the first 200 fs of the pump-probe delay. This is visible in the bottom panel of Figure 2b, such that we did not include this region in the fitting. The fit is overlaid in Figure 2b and the obtained phonon frequencies and dephasing times are reported in **Table 1**. We observe that the 133 cm^{-1} mode decays faster than the 25 cm^{-1} mode, suggesting stronger electron-phonon or phonon-phonon interaction for the 133 cm^{-1} mode.

Figure 2c shows the Fast Fourier transform (FFT) amplitude of the 961 nm line cut together with a low-temperature Raman spectrum. The two dominant frequencies described above coincide with Raman resonances, confirming that the oscillations are not artefacts from our data analysis and belong to the vibrational modes of the material. The absence of resonances in the 50 to 100 cm^{-1} range of the FFT spectrum could be related to the small coupling of these modes to the optical gap of the material.

It is known that the optical properties of Sn-based perovskites are strongly fluence dependent.[2,13,33] The impact of excitation fluence on the 133 cm^{-1} mode is shown in Figure 2d with the ΔT/T residual displayed at two fluences; the inset shows the fitted dephasing time versus excitation fluence. The dephasing time is approximately doubled when the excitation fluence is decreased by a factor of 2.4. When increasing the fluence to 3.1 μJcm^{-2}, see Figure S5a (Supporting Information), the phonon mode is strongly damped. These observations illustrate that the 133 cm^{-1} mode is fluence dependent and is strongly scattered from charge carriers, further illustrating the strong electron–phonon interaction of this mode.

In the following, we will further focus on the importance of the experimental parameters on the coherent phonons. We start our investigation by blue-shifting the pump pulse to 1.44 eV (860 nm), providing 170 meV of extra excess energy with respect to the 980 nm pulses. Figure 2e shows the ΔT/T and ΔT/T residual at a probe wavelength of 972 nm, see Supplementary Figure S6 for the transient absorption map. The increased excess energy provided to the charge carriers reduces the oscillation amplitude of the 133 cm^{-1} mode; it is only after subtracting the electronic dynamics from the ΔT/T signal that the coherent oscillations are observed. The fitting with two damped oscillators results in frequencies of 25 ± 1 cm^{-1} and 138 ± 2 cm^{-1} with dephasing times of 1.1 ± 0.2 ps and 0.6 ± 0.2 ps, respectively. These values are in good agreement with the values obtained for the 980 nm excitation. Only the low-frequency mode is observed when increasing the excitation fluence (Figure S7, Supporting Information). We conclude that the extra kinetic energy of the charge carriers provided by the higher pump photon energy mainly affects the higher frequency mode through additional electron-phonon and phonon-phonon scattering events.

The ΔT/T transient upon a further increase of the excitation photon energy to 3.1 eV (400 nm) and fluence is shown in Figure 2f, see Figure S8 (Supporting Information) for the transient absorption maps. The increased excess energy causes a much slower cooling time to the band edges as the carriers need to dissipate their excess energy through the emission of many phonons. The first stage of the carrier cooling (≈3 ps) results in

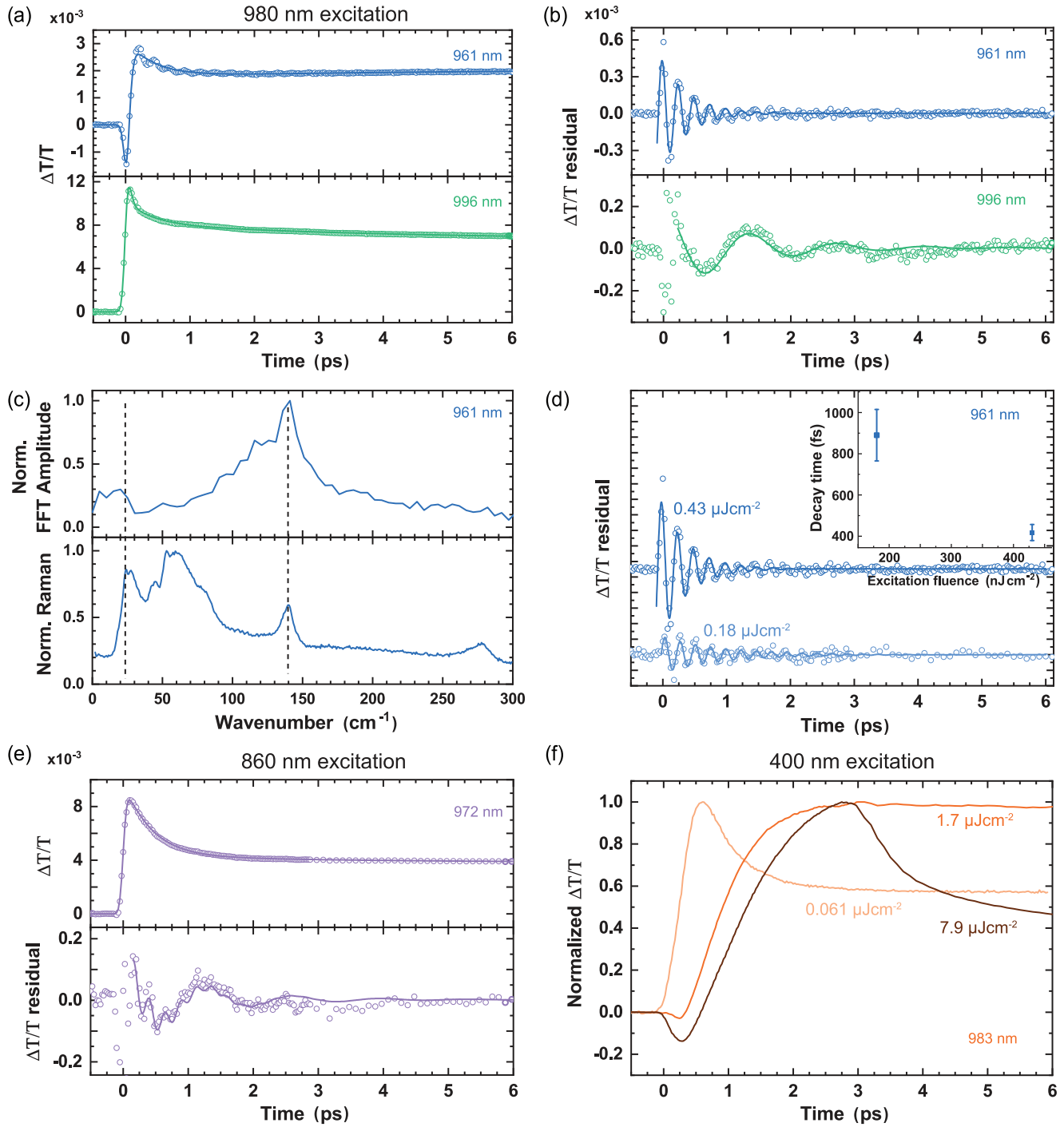

Figure 2. a) Transient absorption dynamics (ΔT/T) at two selected wavelengths of $FASnI_3$ using an 980 nm excitation with a fluence of 0.43 μJcm^{-2}. The data is shown in open circles and the global fit of the electronic dynamics is the full line. b) ΔT/T residual fitted with a damped oscillatory function. c) FFT amplitude compared with Raman spectra. d) ΔT/T residual versus pump-probe delay at two fluences. Inset shows the exponential decay time obtained from fitting with Equation (1). e) ΔT/T at 972 nm (top panel) and ΔT/T residual (bottom panel) excited at 860 nm, fitted with electron dynamics (top panel) and two-term damped sinusoidal function (bottom panel). f) Normalized ΔT/T using 400 nm excitation and probed at 983 nm at different excitation fluences. All measurements were taken at 5 K.

Table 1. Summary of the fitting parameters of Equation (1) to the line cuts of $FASnI_3$ and $CsSnI_3$.

	ω [cm^{-1}]	τ [ps]
$FASnI_3$ 961 nm	133 ± 1	0.42 ± 0.04
$FASnI_3$ 998 nm	25 ± 1	1.2 ± 0.1
$CsSnI_3$ 980 nm	24 ± 1	>>10

non-exponential population decay that is spectrally overlapping with the coherent oscillations. This prevents us from obtaining any reliable ΔT/T residuals from the global fits, as the errors in the fit are larger than the amplitudes of the coherent oscillations. We note that a low excitation fluence of 0.061 μJcm^{-2} (carrier density of ≈2.3 × 10^{16} cm^{-3}) was used, which is lower than the typical fluences needed to observe band edge filling and the hot-phonon bottleneck.[2,3] Increasing the excitation fluence changes the ΔT/T transient in three ways. First, a slower cooling is seen as evidenced by the delayed onset of the ΔT/T maximum. Second, a very fast decay of the ΔT/T transient is observed at fluences >2 μJcm^{-2}, bringing the ΔT/T signal down to ≈4% in ≈2 ps. These non-exponential dynamics were observed for both the 860 and 400 nm excitation wavelength and in both Sn-based compounds. This fast decay is only initiated if a threshold of charge carriers is exceeded. We propose that this fast population decay originates from amplified spontaneous emission, as reported in Pb-based perovskites and organic polymers;[34,35] our hypothesis is supported by the extremely low lasing threshold reported for Sn-based perovskites.[33,36] Third, band edge filling is evidenced as seen by the blue-shifted bleach peak (Figure S8, Supporting Information).

We now broaden our discussion by comparing the results obtained for $FASnI_3$ with $CsSnI_3$. The oscillatory component of the ΔT/T signal for $CsSnI_3$ pumped at 900 nm and probed at 980 nm is shown in **Figure 3a**, see Figure S9 (Supporting Information) for the transient absorption and the ΔT/T residual map. Figure 3a also includes the fit of a sinusoidal function of which the parameters are shown in Table 1. The FFT amplitude of the residual is compared to the Raman spectra in Figure 3b. Two main observations can be drawn. First, only low-frequency modes are observed with the dominant mode at 24 cm^{-1}. Second, the coherent phonon does not show any sign of dephasing up to 8 ps. In addition, this mode does not show faster dephasing by increasing the excitation fluence, as shown in Figure S5b (Supporting Information). In contrast to $FASnI_3$, the long-lived coherent phonon modes of $CsSnI_3$ are observable with 400 nm excitation, as shown in Figure 3c. This indicates the robustness of the phonon mode in $CsSnI_3$, suggesting less scattering from charges and phonons. We underline that the faster phonon decay of the hybrid compound cannot be related to thin film quality as longer PL lifetimes were measured for $FASnI_3$ (Figure S10, Supporting Information).[26] Hence, we conclude that the differences are related to the intrinsic material properties.

It is clear that the A-site cation has a non-negligible impact on the blue-shifted emission from hot carriers. We suggest that its origin lies in the large effect of the A-site cation on the vibrational dynamics, i.e. much shorter phonon dephasing time for $FASnI_3$. This notion is supported by neutron scattering experiments,

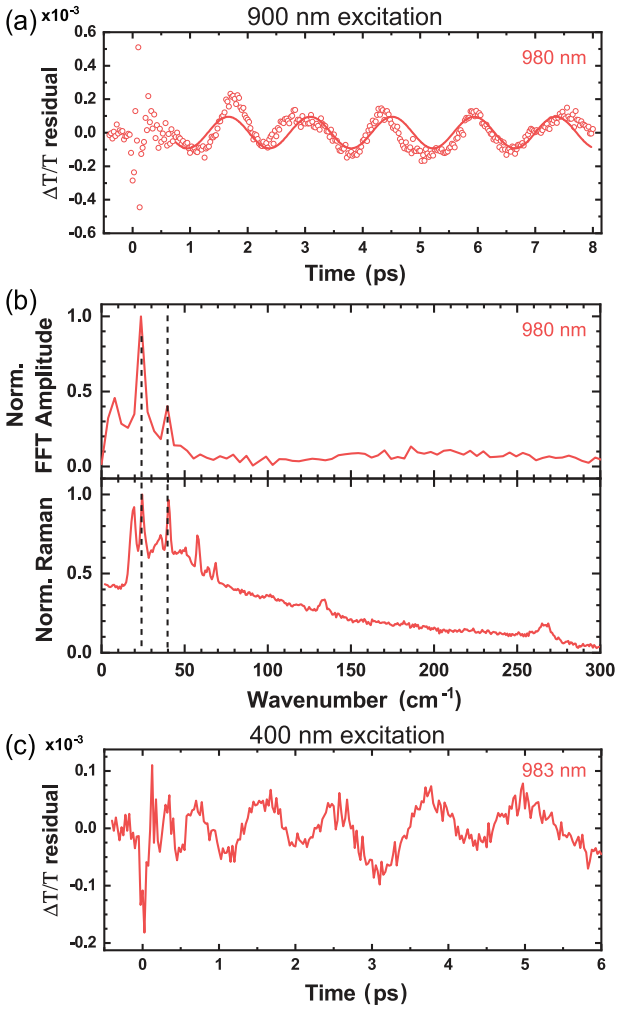

Figure 3. a) ΔT/T residual of $CsSnI_3$ excited at 900 nm with a fluence of 0.28 μJcm^{-2} probed at 980 nm. b) FFT amplitude of ΔT/T residual compared with Raman spectra taken at 5 K. c) ΔT/T residual of $CsSnI_3$ excited at 400 nm with a fluence of 0.23 μJcm^{-2} probed at 983 nm, shortpass FFT filter of 18 THz applied.

which showed that short phonon lifetimes are at the heart of the low thermal conductivity in these compounds and could contribute to the hot-phonon bottleneck.[37–39] In addition, it has been suggested that FA-based compounds show large phonon damping and low sound group velocity, as a result of the coupling between inorganic and organic sub-lattices.[40,41] We propose that the longer phonon dephasing time of $CsSnI_3$ is the signature of a reduced interaction of this optical phonon with other lattice vibrations, and in turn, of the reduced anharmonicity of $CsSnI_3$ compared to $FASnI_3$. The shorter phonon lifetime of $FASnI_3$ means smaller thermal conductivity and slower heat dissipation on the macroscopic length scale, which in turn generates electron reheating and phonon bottleneck. This is in line with reports suggesting the importance of low-energy optical phonon modes in transporting heat in metal halide perovskites.[42] We note that others hypothesised that overlapping phonon density of states would result in stronger phonon–phonon interactions that could facilitate acoustic to optical phonon upconversion and enhance

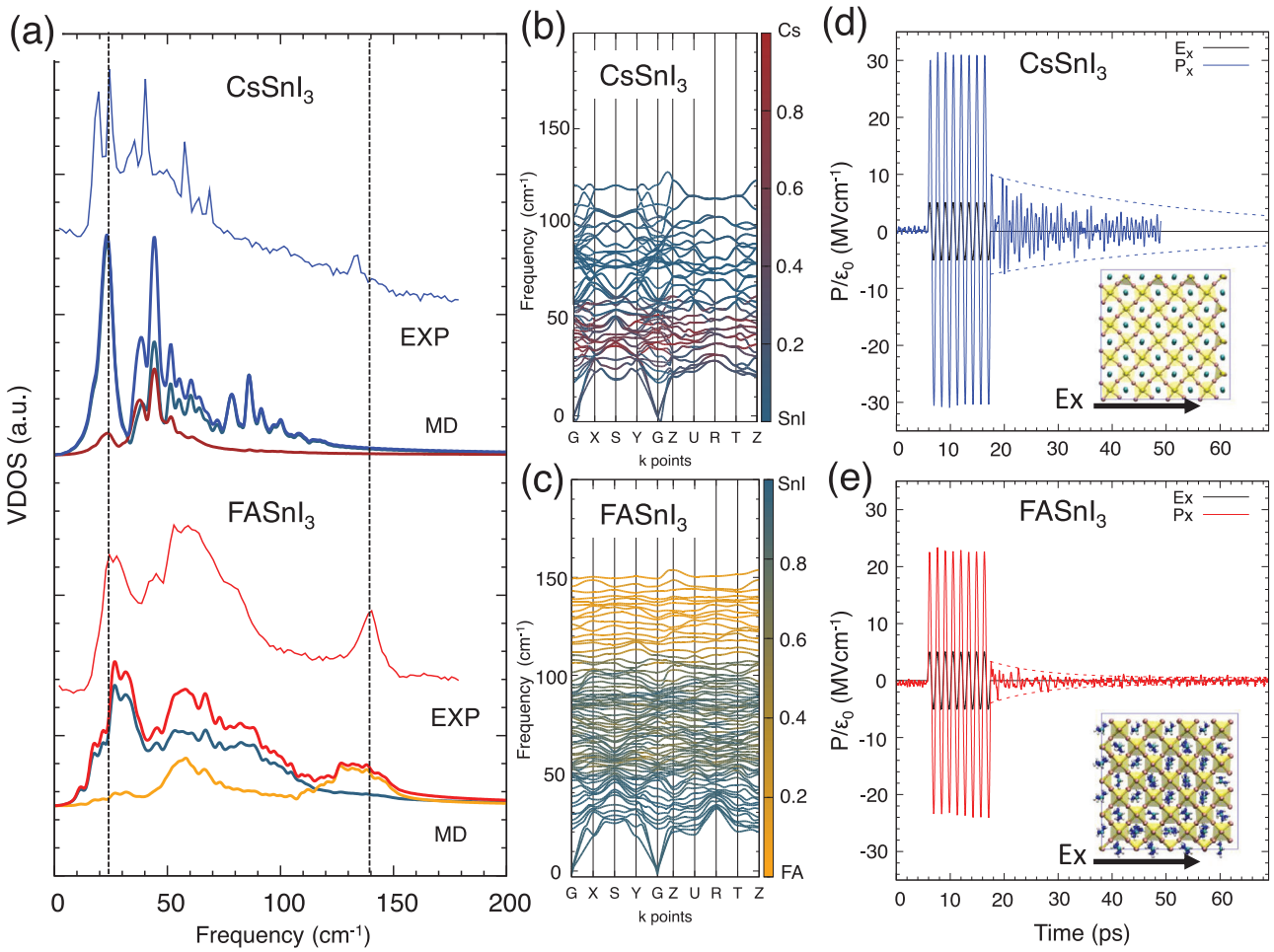

Figure 4. a) Projected vibrational density of states for $CsSnI_3$ (blue) and for $FASnI_3$ (red). Raman spectra are reported for comparison. Steel-blue, brown, and orange lines correspond to SnI, Cs, and FA projections, respectively. Phonon band structure of $CsSnI_3$ b) and $FASnI_3$ c). The color codes are the same as in panel (a). Calculated electric polarization versus time for inorganic d) and hybrid e) crystals induced by a harmonic electric field of 5 $MVcm^{-1}$ (black line). The polarization decays after switching off the field (dashed lines).

the phonon bottleneck.[4] Our observation of faster phonon decay for the hybrid compound is fully consistent with this report. However, we acknowledge that our IVS measurements cannot discriminate the up-converted phonons.

To increase our understanding of these experimental observations, we performed molecular dynamic (MD) simulations. **Figure** 4a shows the projected vibrational density of states (VDOS) calculated for $CsSnI_3$ and $FASnI_3$ along with the Raman spectra obtained by experiments. Two interesting observations can be made: First, the calculated spectra show good agreement with the experimental data, where we see that the 133 cm^{-1} mode described above has a dominant FA character. Second, see also Figure 4b,c, neither of the two compounds shows a phonon bandgap. The absence of the phonon bandgap is independent of the B-site cation, as no significant differences are seen in the VDOS of Pb- and Sn-based perovskites (see Figure S11, Supporting Information). Hence, the long phonon decay time measured for $CsSnI_3$ is not the result of a blockade in the decay of the optical phonon into two acoustic phonons (Klemens decay). Instead, we propose that the optical mode is weakly interacting with other vibrational modes.

To explain the differences in the experimentally measured dephasing times, we performed a simulation based on the application of a harmonic electric field and the corresponding polarisation response of the system.[43] We used a harmonic electric field of 5 $MVcm^{-1}$ with a frequency of 23 cm^{-1} and calculated the polarization as a function of time (see Figure 4d,e). Using this method, we can excite an optical mode that is present in both compounds and track the relaxation over time. After 10 ps of driving the oscillation, the electric field is switched off and the system relaxes to equilibrium, i.e. to a net zero polarization. A clear difference is observed between the compounds with the relaxation time of $CsSnI_3$ being much longer (>40 ps) compared to $FASnI_3$ (≈10 ps), showing the same trend as our experimental data discussed above. This verifies that our model can catch the relevant physics and more insight can be obtained by analyzing the contributions to the relaxation, revealing that the 23 cm^{-1} mode relaxes to a combination of modes in both compounds, albeit a stronger

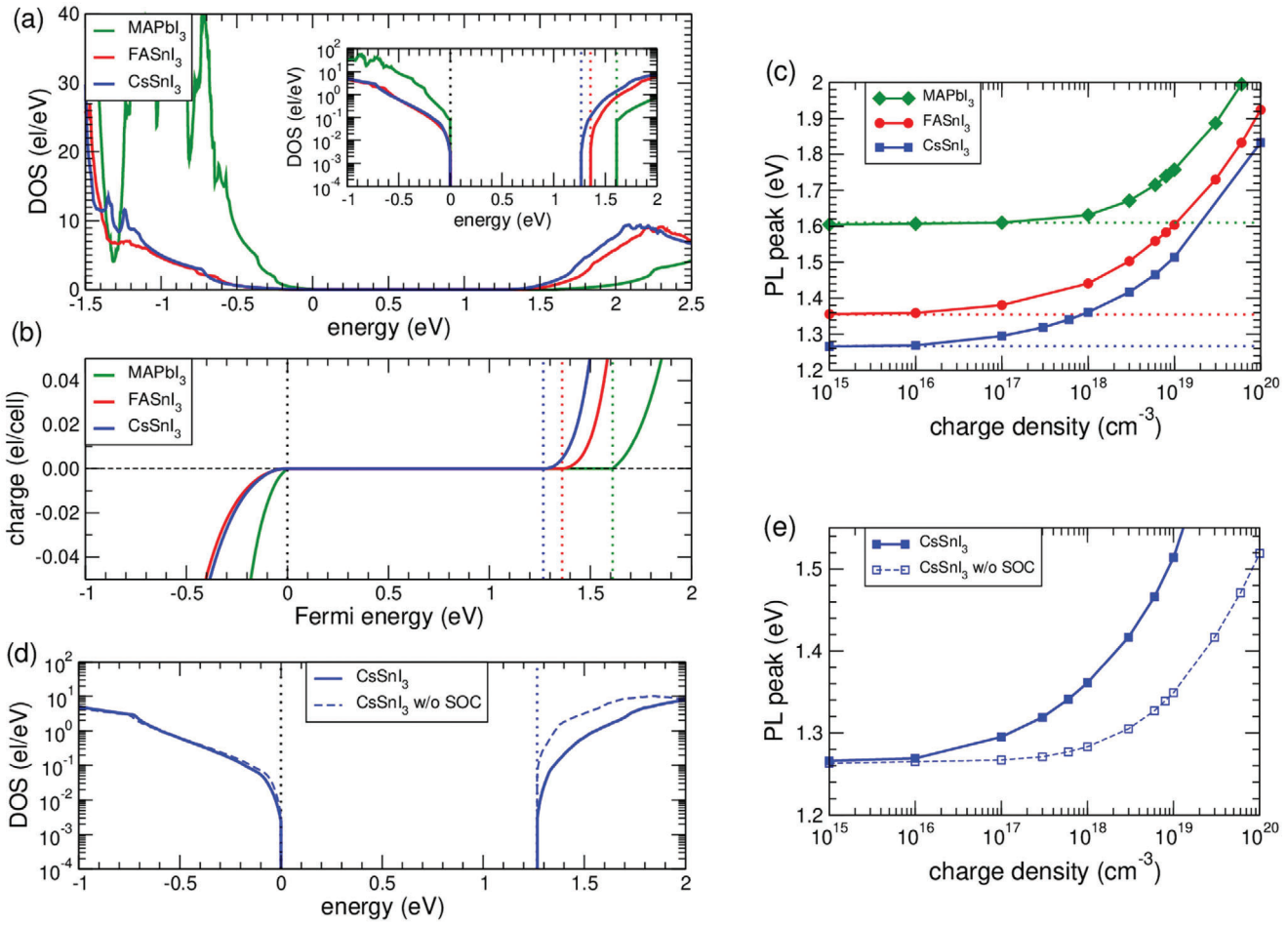

Figure 5. a) Electronic DOS comparison for $MAPbI_3$, $FASnI_3$, $CsSnI_3$. The zero energy is fixed to the VBM. Inset: enlargement around the band extrema; the vertical dotted lines indicate the bandgap. b) Charge (i.e. integrated DOS) versus Fermi energy (zero is fixed to the VBM); positive charge corresponds to electrons in the conduction band and negative charge to holes in the valence. For a given charge injection, the intersecting energies give the associated electron and hole quasi-Fermi levels. c) Calculated PL peak versus injected charge; the horizontal dotted lines indicate the bandgap. d) Electronic DOS and e) PL peak versus injected charge for $CsSnI_3$ with and without spin-orbit coupling.

interaction and faster decay time is obtained for $FASnI_3$. This observation is consistent with the much broader Raman linewidths (both simulations and experiments) obtained for $FASnI_3$ compared to the sharper peaks of $CsSnI_3$. This is also consistent with the fact that molecules provide additional degrees of freedom at low temperatures that favor the mixing of phonon modes and scattering of phonons.[44]

The shorter dephasing time observed in the hybrid $FASnI_3$ compared to the inorganic $CsSnI_3$ crystal can be attributed to anharmonic and anisotropic interactions between the molecule and the SnI lattice. In particular, we identify the hydrogen H–I bonding at the origin of the faster relaxation and dephasing in the hybrid case. This conclusion is obtained by a toy model of the hybrid crystal in which we remove the hydrogen atoms from the formamidinium molecules, see discussion Supporting Information and Figure S12 (Supporting Information).

One aspect of our MD calculations is the similar VDOS of Sn- and Pb-based compounds (Figure S11, Supporting Information). The vibrational properties can therefore not account for the experimentally observed differences between the blueshift of Pb and Sn. We will show in the following that the shift is mainly determined by the electronic properties of the Sn cation.

In **Figure 5a** we report the electronic DOS calculated including spin-orbit coupling (SOC) for $CsSnI_3$, $FASnI_3$, and $MAPbI_3$. As expected, the Sn-based perovskites have a smaller bandgap than the Pb-based system. In addition, the conduction band minimum (CBM) and valence band maximum (VBM) of the Sn-based perovskites are very similar as the A-site cations do not contribute directly to the valence band edges and lie deep in the electronic bands.[22,45] When comparing $MAPbI_3$ with the Sn-based perovskites, we observe that the DOS at the CBM shows a similar gradual increase at the onset. In contrast, for $MAPbI_3$ the DOS increase at the VBM is much steeper than for stannates. This is a consequence of the more dispersed 5s valence states of stannates with respect to the corresponding 6s states of $MAPbI_3$. In the inset the logarithmic scale is shown to highlight the DOS detail around the bandgap; notice the step-like shape of $MAPbI_3$ at the extrema, owing to the strong Rashba effect.

The result of this DOS difference visually translates into the charge carrier versus Fermi energy shown in Figure 5b: for fixed

electron and hole quasi-Fermi levels, the smoother the DOS at the band edges, the smaller the charge that can be hosted in the bands. Hence, due to the tiny DOS of the Sn-based perovskites, the electron–hole chemical potential must rise sharply when large carrier densities are injected (Figure S15, Supporting Information), resulting in a giant band-filling effect and dynamic Burstein–Moss shift for stannates. As an example, hosting an injected charge of ≈0.01 electrons per cell, corresponding to a charge carrier density of 10^{19} cm^{-3}, requires an electron-hole chemical potential shift (i.e. energy in excess of the bandgap) of 324 meV in $CsSnI_3$. On the other hand, only about half of this shift is required for $MAPbI_3$. This chemical potential shift reverberates into the PL peak, calculated as a function of the carrier density in Figure 5c. The peak position rises at a much faster pace for stannates than for plumbates; in other words, the Burstein–Moss shift, while still remarkable for $MAPbI_3$, is not nearly as large as for stannates. The comparison with the experimental data in Figure 1d shows that our theoretical approach is capable of reproducing the observed material-dependent trend and also predicts a peak shift magnitude in satisfying agreement with the measured values.

Ultimately, the giant Burstein–Moss effect can be traced back to the very peculiar electronic properties at the band edges of stannates. To this point, it is worth emphasizing the fundamental role played by SOC in halide perovskites: in Figure 5d we compare the $CsSnI_3$ DOS with and without SOC (similar results are found for $FASnI_3$, see Figure S16, Supporting Information). We observe that SOC greatly affects the conduction band, generating a much smoother DOS at the CBM with respect to the SOC-free band structure counterpart. Thus, SOC is not only relevant to the bandgap value but also to the DOS shape and is essential to the generation of a giant Burstein–Moss shift in Sn perovskites. In Figure 5e we report the comparison of the PL shift for $CsSnI_3$ with and without SOC: taking again a carrier density of 10^{19} cm^{-3} as a reference, we obtain a PL peak shift of 250 and 90 meV for the two curves, respectively. In turn, the low DOS at the band edges is motivated by highly dispersive bands and low effective masses, as shown in Figure S17 (Supporting Information). We notice that the connection between tiny DOS at the band edges and hot-carrier behaviour was already proposed for plumbates.[46] Strikingly, we find this effect to be amplified for stannates. This is also reflected in the calculated absorption coefficient, reported in Figure S18 (Supporting Information): the smaller DOS at the band extrema for stannates causes a visibly smaller cross-section at the onset.

Our results naturally spark the discussion about how hot the carriers are in metal halide perovskites as we point to a Burnstein–Moss-dominated mechanism. While the large blue shift can be well accounted for with Burstein–Moss effects, the high-energy tail of the emission is evidence for hot-carrier recombination.[2,22] The fact that both of these mechanisms are present could lead to erroneous values of the carrier temperatures and validates the question of whether the carriers are "hot or not." Creating an elaborate model that provides correct values is beyond the scope of our work, although models have been reported in the literature.[6] While this semantic discussion is important, we underline that in our case carriers have not lost their energy and this energy can still be extracted in a device, at least in principle. So whether the carriers are hot or have high energy because the lower states are occupied, the final purpose of the high-efficiency solar cells we are aiming for remains within sight.

Our results reveal that the dispersion at the band edges is instrumental to hot-carrier behavior and should be taken into account as a crucial ingredient for the design of innovative solar cell architectures and the search for new hot-carrier materials with high throughput computational studies. In this way, we can expand previous theoretical works focusing mainly on material systems with large phonon bandgaps by also considering the dispersion at the band edge. We are confident that this approach will accelerate the prospective of a high-efficiency hot-carrier solar cell.

3. Conclusion

In summary, we fabricated $FASnI_3$ and $CsSnI_3$ thin films of comparable quality and performed an in-depth analysis of the slow cooling observed in tin halide perovskites. We show that the blue-shifted PL at high excitation fluences is the result of the summation of several physical contributions, where the larger shift of $FASnI_3$ compared to $CsSnI_3$ is correlated with faster dephasing times of its vibrational modes. Hence, the phonons of the hybrid perovskite scatter much stronger compared to the fully inorganic system. However, the vibrational behavior cannot account for the different blueshifts observed between Sn- and Pb-based perovskites. Through electronic band calculations, we show that the band filling is at the origin of the long hot-carrier lifetimes due to a peculiarly small DOS at the band edges for Sn-based perovskites. Our analysis reveals design principles for new hot-carrier materials and solidifies our understanding of hot-carrier dynamics.

Supporting Information

Supporting Information is available from the Wiley Online Library or from the author.

Acknowledgements

The authors kindly thank A.F. Kamp and T. Zaharia for their technical support. This work was financed through the Materials for Sustainability (Mat4Sus) programme (739.017.005) of the Netherlands Organisation for Scientific Research (NWO) E.K.T. acknowledges the financial support of the Zernike Institute of Advanced Materials Bonus Incentive Scheme and LASERLAB-EUROPE (PID: 20263). A.M. acknowledges New Energy and Industrial Technology Development Organization (NEDO, Japan), computational support from CINECA (Italy) through the ISCRA initiative, and European Union Next Generation EU for funding through "ICSC - Centro Nazionale HPC" Project B93C22000620006 and MUR Projects PRIN 2022 "NEWATOMISTS" B53D23004630006 and PRIN PNRR 2022"ORIENTING" B53D23025530001. A.F. acknowledges project NEST funded under the National Recovery and Resilience Plan (NRRP), Mission 4 Component 2 Investment 1.3 - Call for tender No. 1561 of 11.10.2022 of Ministero dell'Università e della Ricerca (MUR); funded by the European Union Next Generation EU.

Conflict of Interest

The authors declare no conflict of interest.

Author Contributions

E.K.T. contributed to conceptualization, formal analysis, funding acquisition, investigation, and writing the original draft; F.V.A.C. participated in investigation and writing (review and editing); A.F. was involved in formal analysis and writing (review and editing); A.M. contributed to formal analysis and writing (review and editing); L.v.d.V. provided resources and participated in writing (review and editing); M.P. contributed resources; G.C. provided supervision and participated in writing (review and editing); and M.A.L. contributed to conceptualization, supervision, writing (review and editing), and funding acquisition.

Data Availability Statement

The data that support the findings of this study are available from the corresponding author upon reasonable request.

Keywords

hot carriers, impulsive vibrational spectroscopy, molecular dynamics, photophysics, tin perovskite

Received: August 12, 2024
Revised: November 5, 2024
Published online: December 11, 2024

[1] W. Shockley, H. J. Queisser, *J. Appl. Phys.* **1961**, *32*, 510.
[2] H. H. Fang, S. Adjokatse, S. Shao, J. Even, M. A. Loi, *Nat. Commun.* **2018**, *9*, 243.
[3] Y. Yang, D. P. Ostrowski, R. M. France, K. Zhu, J. Van De Lagemaat, J. M. Luther, M. C. Beard, *Nat. Photonics* **2016**, *10*, 53.
[4] J. Yang, X. Wen, H. Xia, R. Sheng, Q. Ma, J. Kim, P. Tapping, T. Harada, T. W. Kee, F. Huang, Y. B. Cheng, M. Green, A. Ho-Baillie, S. Huang, S. Shrestha, R. Patterson, G. Conibeer, *Nat. Commun.* **2017**, *8*, 14120.
[5] H. Zhu, K. Miyata, Y. Fu, J. Wang, P. P. Joshi, D. Niesner, K. W. Williams, S. Jin, X. Y. Zhu, *Science* **2016**, *353*, 1409.
[6] K. J. Savill, M. T. Klug, R. L. Milot, H. J. Snaith, L. M. Herz, *J. Phys. Chem. Lett.* **2019**, *10*, 6038.
[7] J. S. Manser, P. V. Kamat, *Nat. Photonics* **2014**, *8*, 737.
[8] T. R. Hopper, A. Gorodetsky, J. M. Frost, C. Müller, R. Lovrincic, A. A. Bakulin, *ACS Energy Lett.* **2018**, *3*, 2199.
[9] B. P. Carwithen, T. R. Hopper, Z. Ge, N. Mondal, T. Wang, R. Mazlumian, X. Zheng, F. Krieg, F. Montanarella, G. Nedelcu, M. Kroll, M. A. Siguan, J. M. Frost, K. Leo, Y. Vaynzof, M. I. Bodnarchuk, M. V. Kovalenko, A. A. Bakulin, *ACS Nano* **2023**, *17*, 6638.
[10] D. W. Dequilettes, K. Frohna, D. Emin, T. Kirchartz, V. Bulovic, D. S. Ginger, S. D. Stranks, *Chem. Rev.* **2019**, *119*, 11007.
[11] S. Kahmann, M. A. Loi, *J. Mater. Chem. C.* **2019**, *7*, 2471.
[12] M. Li, J. Fu, Q. Xu, T. C. Sum, *Adv. Mater.* **2019**, *31*, 1802486.
[13] L. J. M. van de Ven, E. K. Tekelenburg, M. Pitaro, J. Pinna, M. A. Loi, *ACS Energy Lett.* **2024**, *9*, 992.
[14] M. Liebel, C. Schnedermann, T. Wende, P. Kukura, *J. Phys. Chem. A* **2015**, *119*, 9506.
[15] G. Batignani, G. Fumero, A. R. Srimath Kandada, G. Cerullo, M. Gandini, C. Ferrante, A. Petrozza, T. Scopigno, *Nat. Commun.* **2018**, *9*, 1971.
[16] F. Thouin, D. A. Valverde-Chávez, C. Quarti, D. Cortecchia, I. Bargigia, D. Beljonne, A. Petrozza, C. Silva, A. R. Srimath Kandada, *Nat. Mater.* **2019**, *18*, 349.
[17] J. Fu, M. Li, A. Solanki, Q. Xu, Y. Lekina, S. Ramesh, Z. X. Shen, T. C. Sum, *Adv. Mater.* **2021**, *33*, 2006233.
[18] P. Maity, J. Yin, B. Cheng, J. H. He, O. M. Bakr, O. F. Mohammed, *J. Phys. Chem. Lett.* **2019**, *10*, 5259.
[19] D. M. Monahan, L. Guo, J. Lin, L. Dou, P. Yang, G. R. Fleming, *J. Phys. Chem. Lett.* **2017**, *8*, 3211.
[20] S. Tao, I. Schmidt, G. Brocks, J. Jiang, I. Tranca, K. Meerholz, S. Olthof, *Nat. Commun.* **2019**, *10*, 2560.
[21] R. L. Milot, M. T. Klug, C. L. Davies, Z. Wang, H. Kraus, H. J. Snaith, M. B. Johnston, L. M. Herz, *Adv. Mater.* **2018**, *30*.
[22] A. Filippetti, S. Kahmann, C. Caddeo, A. Mattoni, M. Saba, A. Bosin, M. A. Loi, *J. Mater. Chem. A* **2021**, *9*, 11812.
[23] U. Bockelmann, G. Bastard, *Phys. Rev. B* **1990**, *42*, 8947.
[24] G. J. Conibeer, D. König, M. A. Green, J. F. Guillemoles, *Thin Solid Films* **2008**, *516*, 6948.
[25] J. Fu, Q. Xu, G. Han, B. Wu, C. H. A. Huan, M. L. Leek, T. C. Sum, *Nat. Commun.* **2017**, *8*, 1300.
[26] S. Kahmann, S. Shao, M. A. Loi, *Adv. Funct. Mater.* **2019**, *29*, 1.
[27] L. Dai, J. Ye, N. C. Greenham, *Light: Sci. Appl.* **2023**, *12*, 208.
[28] M. Righetto, S. S. Lim, D. Giovanni, J. W. M. Lim, Q. Zhang, S. Ramesh, Y. K. E. Tay, T. C. Sum, *Nat. Commun.* **2020**, *11*, 1.
[29] T. Ghosh, S. Aharon, A. Shpatz, L. Etgar, S. Ruhman, *ACS Nano* **2018**, *12*, 5719.
[30] M. B. Price, J. Butkus, T. C. Jellicoe, A. Sadhanala, A. Briane, J. E. Halpert, K. Broch, J. M. Hodgkiss, R. H. Friend, F. Deschler, *Nat. Commun.* **2015**, *6*, 1.
[31] J. J. Snellenburg, S. Laptenok, R. Seger, K. M. Mullen, I. H. M. van Stokkum, *J. Stat. Softw.* **2012**, *49*, 1.
[32] H. Wang, L. Valkunas, T. Cao, L. Whittaker-Brooks, G. R. Fleming, *J. Phys. Chem. Lett.* **2016**, *7*, 3284.
[33] G. Xing, M. H. Kumar, W. K. Chong, X. Liu, Y. Cai, H. Ding, M. Asta, M. Grätzel, S. Mhaisalkar, N. Mathews, T. C. Sum, *Adv. Mater.* **2016**, *28*, 8191.
[34] G. Xing, N. Mathews, S. S. Lim, N. Yantara, X. Liu, D. Sabba, M. Grätzel, S. Mhaisalkar, T. C. Sum, *Nat. Mater.* **2014**, *13*, 476.
[35] G. Cerullo, S. Stagira, M. Nisoli, S. De Silvestri, G. Lanzani, *Phys. Rev. B: Condens. Matter Mater. Phys.* **1998**, *57*, 12806.
[36] R. L. Milot, G. E. Eperon, T. Green, H. J. Snaith, M. B. Johnston, L. M. Herz, *J. Phys. Chem. Lett.* **2016**, *7*, 4178.
[37] B. Li, Y. Kawakita, Y. Liu, M. Wang, M. Matsuura, K. Shibata, S. Ohira-Kawamura, T. Yamada, S. Lin, K. Nakajima, S. F. Liu, *Nat. Commun.* **2017**, *8*, 16086.
[38] A. M. Leguy, J. M. Frost, A. P. McMahon, V. G. Sakai, W. Kochelmann, C. Law, X. Li, F. Foglia, A. Walsh, B. C. O'Regan, J. Nelson, J. T. Cabral, P. R. Barnes, *Nat. Commun.* **2015**, *6*, 7124.
[39] W. Lee, H. Li, A. B. Wong, D. Zhang, M. Lai, Y. Yu, Q. Kong, E. Lin, J. J. Urban, J. C. Grossman, P. Yang, *Proc. Natl. Acad. Sci. USA* **2017**, *114*, 8693.
[40] A. C. Ferreira, A. Létoublon, S. Paofai, S. Raymond, C. Ecolivet, B. Rufflé, S. Cordier, C. Katan, M. I. Saidaminov, A. A. Zhumekenov, O. M. Bakr, J. Even, P. Bourges, *Phys. Rev. Lett.* **2018**, *121*, 085502.
[41] A. C. Ferreira, S. Paofai, A. Létoublon, J. Ollivier, S. Raymond, B. Hehlen, B. Rufflé, S. Cordier, C. Katan, J. Even, P. Bourges, *Commun. Phys.* **2020**, *3*, 48.
[42] A. Gold-Parker, P. M. Gehring, J. M. Skelton, I. C. Smith, D. Parshall, J. M. Frost, H. I. Karunadasa, A. Walsh, M. F. Toney, *Proc. Natl. Acad. Sci. USA* **2018**, *115*, 11905.
[43] A. Mattoni, C. Caddeo, *J. Chem. Phys.* **2020**, *152*, 104705.
[44] C. Caddeo, C. Melis, M. I. Saba, A. Filippetti, L. Colombo, A. Mattoni, *Phys. Chem. Chem. Phys.* **2016**, *18*, 24318.
[45] I. Borriello, G. Cantele, D. Ninno, *Phys. Rev. B: Condens. Matter Mater. Phys.* **2008**, *77*, 235214.
[46] H. Kawai, G. Giorgi, A. Marini, K. Yamashita, *Nano Lett.* **2015**, *15*, 3103.